




# Functional and Structural Insights into a Vif/PPP2R5 Complex Elucidated Using Patient HIV-1 Isolates and Computational Modeling

 Daniel J. Salamango,<sup>a,b,c</sup> Jennifer L. McCann,<sup>a,b,c,d</sup> Özlem Demir,<sup>f</sup> Jordan T. Becker,<sup>a,b,c</sup> Jiayi Wang,<sup>a,b,c,e</sup> Jairam R. Lingappa,<sup>g,h,i</sup> Nuri A. Temiz,<sup>a,b,c</sup> William L. Brown,<sup>a,b,c</sup> Rommie E. Amaro,<sup>f</sup>  Reuben S. Harris<sup>a,b,c,d</sup>

<sup>a</sup>Department of Biochemistry, Molecular Biology and Biophysics, University of Minnesota, Minneapolis, Minnesota, USA

<sup>b</sup>Masonic Cancer Center, University of Minnesota, Minneapolis, Minnesota, USA

<sup>c</sup>Institute for Molecular Virology, University of Minnesota, Minneapolis, Minnesota, USA

<sup>d</sup>Howard Hughes Medical Institute, University of Minnesota, Minneapolis, Minnesota, USA

<sup>e</sup>Department of Virology and Infectious Disease, Rockefeller University, New York, New York, USA

<sup>f</sup>Department of Chemistry and Biochemistry, University of San Diego, La Jolla, California, USA

<sup>g</sup>Department of Global Health, University of Washington, Seattle, Washington, USA

<sup>h</sup>Department of Medicine, University of Washington, Seattle, Washington, USA

<sup>i</sup>Department of Pediatrics, University of Washington, Seattle, Washington, USA

**ABSTRACT** Human immunodeficiency virus type 1 (HIV-1) Vif recruits a cellular ubiquitin ligase complex to degrade antiviral APOBEC3 enzymes (APOBEC3C-H) and PP2A phosphatase regulators (PPP2R5A to PPP2R5E). While APOBEC3 antagonism is the canonical function of HIV-1 Vif, this viral accessory protein is also known to trigger G<sub>2</sub>/M cell cycle arrest. Vif initiates G<sub>2</sub>/M arrest by degrading multiple PPP2R5 family members, an activity prevalent among diverse HIV-1 and simian immunodeficiency virus (SIV) isolates. Here, computational protein-protein docking was used to delineate a Vif/CBF- $\beta$ /PPP2R5 complex in which Vif is predicted to bind the same PPP2R5 surface as physiologic phosphatase targets. This model was tested using targeted mutagenesis of amino acid residues within or adjacent to the putative interface to show loss or retention, respectively, of Vif-induced PPP2R5 degradation activity. Additionally, expression of a peptide that mimics cellular targets of PPP2R5s robustly inhibited Vif-mediated degradation of PPP2R5A but not APOBEC3G. Moreover, live-cell imaging studies examining Vif-mediated degradation of PPP2R5A and APOBEC3G within the same cell revealed that PPP2R5A degradation kinetics are comparable to those of APOBEC3G with a half-life of roughly 6 h postinfection, demonstrating that Vif can concurrently mediate the degradation of distinct cellular substrates. Finally, experiments with a panel of patient-derived Vif isolates indicated that PPP2R5A degradation activity is common in patient-derived isolates. Taken together, these results support a model in which PPP2R5 degradation and global changes in the cellular phosphoproteome are likely to be advantageous for viral pathogenesis.

**IMPORTANCE** A critical function of HIV-1 Vif is to counteract the family of APOBEC3 innate immune proteins. It is also widely accepted that Vif induces G<sub>2</sub>/M cell cycle arrest in several different cell types. Recently, it has been shown that Vif degrades multiple PPP2R5 phosphoregulators to induce the G<sub>2</sub>/M arrest phenotype. Here, computational approaches are used to test a structural model of the Vif/PPP2R5 complex. In addition, imaging studies are used to show that Vif degrades these PPP2R5 substrates in roughly the same time frame as APOBEC3 degradation and that this activity is prevalent in patient-derived Vif isolates. These studies are important by further defining PPP2R5 proteins as a bona fide substrate of HIV-1 Vif.

**Citation** Salamango DJ, McCann JL, Demir Ö, Becker JT, Wang J, Lingappa JR, Temiz NA, Brown WL, Amaro RE, Harris RS. 2020. Functional and structural insights into a Vif/PPP2R5 complex elucidated using patient HIV-1 isolates and computational modeling. *J Virol* 94:e00631-20. <https://doi.org/10.1128/JVI.00631-20>.

**Editor** Frank Kirchoff, Ulm University Medical Center

**Copyright** © 2020 American Society for Microbiology. All Rights Reserved.

Address correspondence to Daniel J. Salamango, [dsalaman@umn.edu](mailto:dsalaman@umn.edu), or Reuben S. Harris, [rsh@umn.edu](mailto:rsh@umn.edu).

**Received** 6 April 2020

**Accepted** 17 August 2020

**Accepted manuscript posted online** 26 August 2020

**Published** 14 October 2020

**KEYWORDS** Vif, HIV-1, PPP2R5, Vif, host-pathogen interaction, phosphatase regulation

The best-known function of HIV-1 Vif is to counteract the mutagenic potential of the APOBEC3 family of DNA cytosine deaminases (reviewed in references 1–4). Vif achieves this by nucleating the formation of a CBF- $\beta$ , ELOB/C, CUL5, and RBX2 E3 ubiquitin ligase complex to degrade restrictive APOBEC3s (5, 6). In the absence of Vif, APOBEC3G, APOBEC3F, APOBEC3D, and APOBEC3H can package into nascent HIV-1 particles and generate C-to-U lesions in the viral cDNA, causing nonsense mutations, missense mutations, and abortive integration. Several APOBEC3 enzymes also exert deaminase-independent antiviral activities and hinder reverse transcription, likely through high affinities for RNA and single-stranded-DNA viral replication intermediates (7, 8).

Another ascribed Vif function is its ability to promote G<sub>2</sub>/M cell cycle arrest in adherent, myeloid, and lymphoid cell lines (9–13). Recent quantitative proteomic studies of HIV-1-infected T cells identified new Vif substrates, including multiple members of the PPP2R5 family of protein phosphatase 2A (PP2A) regulators (14, 15). PP2A enzymes function as heterotrimeric complexes comprising a phosphatase enzyme (PP2C $\alpha$ ), a scaffolding protein (PPP2R1 $\alpha$  or PPP2R1 $\beta$ ), and a regulatory (B) subunit (16–19). The B subunit is from one of three different protein families (B55 $\alpha$ - $\delta$ , B' [PPP2R5A-E], or B'' [PR72/130]), and it serves to regulate the subcellular localization and substrate specificity of each PP2A holoenzyme complex (16, 20). Our group recently demonstrated an inextricable relationship between PPP2R5 degradation by HIV-1 Vif and G<sub>2</sub>/M cell cycle arrest (21). Critical studies included the delineation of an electrostatic interface at the core of the interaction and global bioinformatic analysis indicating that these activities are prevalent among diverse HIV-1 subtypes.

Here, protein-protein docking and targeted mutagenesis experiments were used to generate and validate a structural model for the Vif/CBF- $\beta$ /PPP2R5 holo-complex. Single-amino-acid substitutions within the predicted interface could disrupt Vif-mediated degradation of PPP2R5A, whereas substitutions at positions immediately adjacent to the interface had minimal impact. In further support of this model, a peptide inhibitor that is known to bind the same PPP2R5 surface as the predicted Vif interface could disrupt degradation of PPP2R5A but not APOBEC3G. Furthermore, degradation kinetics were established for APOBEC3G and PPP2R5A substrates within the same cells following infection with Vif-proficient or -deficient virus. Following virus infection, the half-life of PPP2R5A was observed to be roughly 6 h, which is comparable to the 4-h half-life of APOBEC3G. Finally, functional studies indicate that roughly half of the patient-derived Vif isolates tested are capable of inducing PPP2R5 degradation, that this activity is prevalent both in samples where virus transmission did and did not occur, and that it is observed at a higher frequency than degradation of the potent restrictor APOBEC3H. Taken together, these results suggest that degradation of PPP2R5s is advantageous for viral pathogenesis.

## RESULTS

**Modeling a Vif/PPP2R5 complex.** Obtaining structural information for Vif/substrate complexes has proven challenging, with no cocrystal structures and only one cryo-electron microscopy report of a partial HIV-1 Vif/CBF- $\beta$ /APOBEC3F ternary complex (22). To overcome this limitation, computational protein-protein docking (PPD) was used to generate a structural model to better understand how Vif binds to PPP2R5 substrates (Fig. 1). Using 10 previously identified amino acid residues required for PPP2R5 degradation as anchor points (21), PPD was used to generate 30 independent models of a Vif/CBF- $\beta$ /PPP2R5 complex (PPP2R5C was used for modeling [PDB code 2IAE]; for an example, see Fig. 1A). CBF- $\beta$  was included in these docking experiments because it is critical for Vif stability *in vivo* and essential for APOBEC3 degradation as well as degradation of PPP2R5 proteins and G<sub>2</sub>/M arrest (6, 13, 14). Of the models

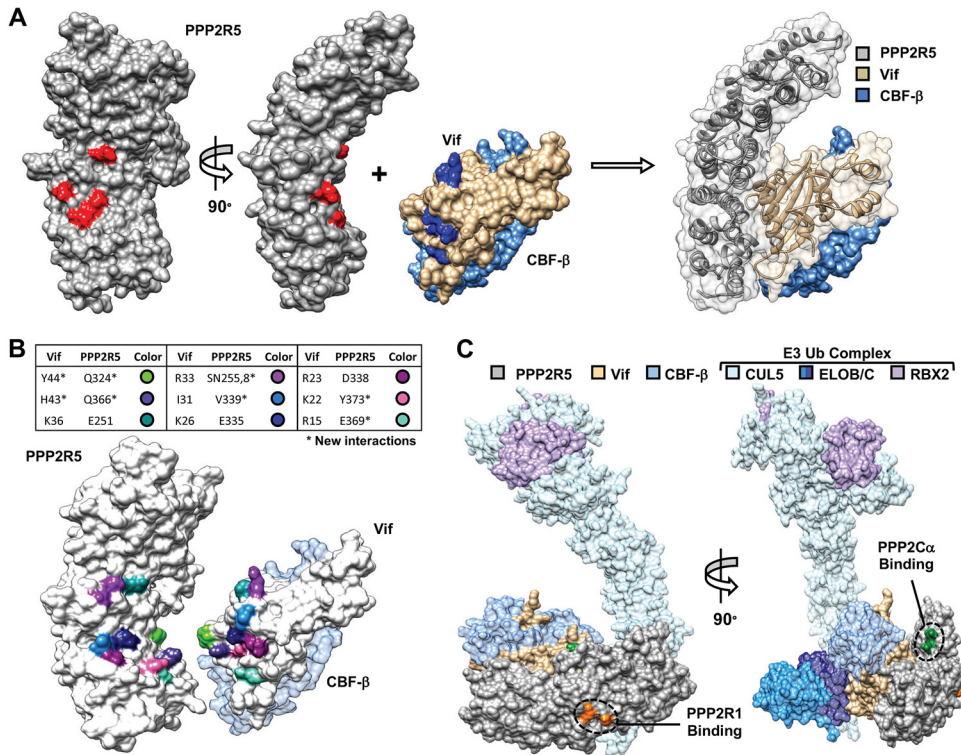


**FIG 1** Model of a Vif/CBF- $\beta$ /PPP2R5 complex. (A) Surface representation of PPP2R5C (PDB code 2IAE) and Vif/CBF- $\beta$  (PDB code 4N9F) used in protein-protein docking simulations to generate the depicted complex. Residues highlighted in red (negatively charged amino acids) and blue (positively charged amino acids) represent positions identified previously as being important for Vif-mediated degradation of PPP2R5A and were used here as anchor points for docking simulations. (B) Depiction of the amino acid residue pairings between PPP2R5 and Vif implicated in forming the protein-protein interface. PPP2R5 amino acids are based on the 5A family member. (C) Model of a PPP2R5 substrate docked onto the X-ray structure of Vif in complex with the E3-ubiquitin ligase complex (PDB code 4N9F).

generated, one had all anchor residues contained within a putative Vif/CBF- $\beta$ /PPP2R5 interface and was therefore selected for further investigation. The interface defined by this PPD model includes 9 novel amino acid residues not implicated by prior studies (2 from Vif and 7 from PPP2R5) (Fig. 1B) (21). Interestingly, 17 of 19 residues within the putative interface are polar or charged, with 4 of the residue pairings predicted to form salt bridges (Fig. 1B). Importantly, no steric clashing is observed when the Vif/CBF- $\beta$ /PPP2R5 model is overlaid onto an X-ray crystal structure of a substrate-free Vif/CBF- $\beta$ /ELOB/ELOC/CUL5 complex (Fig. 1C) (5). Additionally, the model of the full Vif/PPP2R5/E3-ubiquitin ligase complex suggests that the surface bound by Vif is solvent exposed and does not interfere with PPP2C $\alpha$  or PPP2R1 $\alpha/\beta$  interfaces used to form a functional trimeric phosphatase complex (Fig. 1C) (20).

**Testing the Vif/PPP2R5 model.** To interrogate the Vif/PPP2R5 structural model, amino acid substitutions were generated at newly identified PPP2R5 and Vif positions that were predicted to engage in electrostatic interactions or that appeared to have spatial constraints (Fig. 2A and B). 293T cells stably expressing either wild-type or mutant enhanced green fluorescent protein (eGFP)-tagged PPP2R5A proteins were transfected with an mCherry-T2A-Vif expression plasmid containing either wild-type IIIIB Vif or the appropriate Vif variants, and degradation was assessed via flow cytometry (as loss of eGFP fluorescence in mCherry-positive cells). In support of the model, introducing either charged (Arg or Lys) or bulky hydrophobic (Trp) amino acid residues at newly identified PPP2R5A positions predicted to form the putative Vif interface severely abrogated degradation (Fig. 2A and C, top histograms). However, similar substitutions targeting amino acid residues predicted to be immediately adjacent to the putative

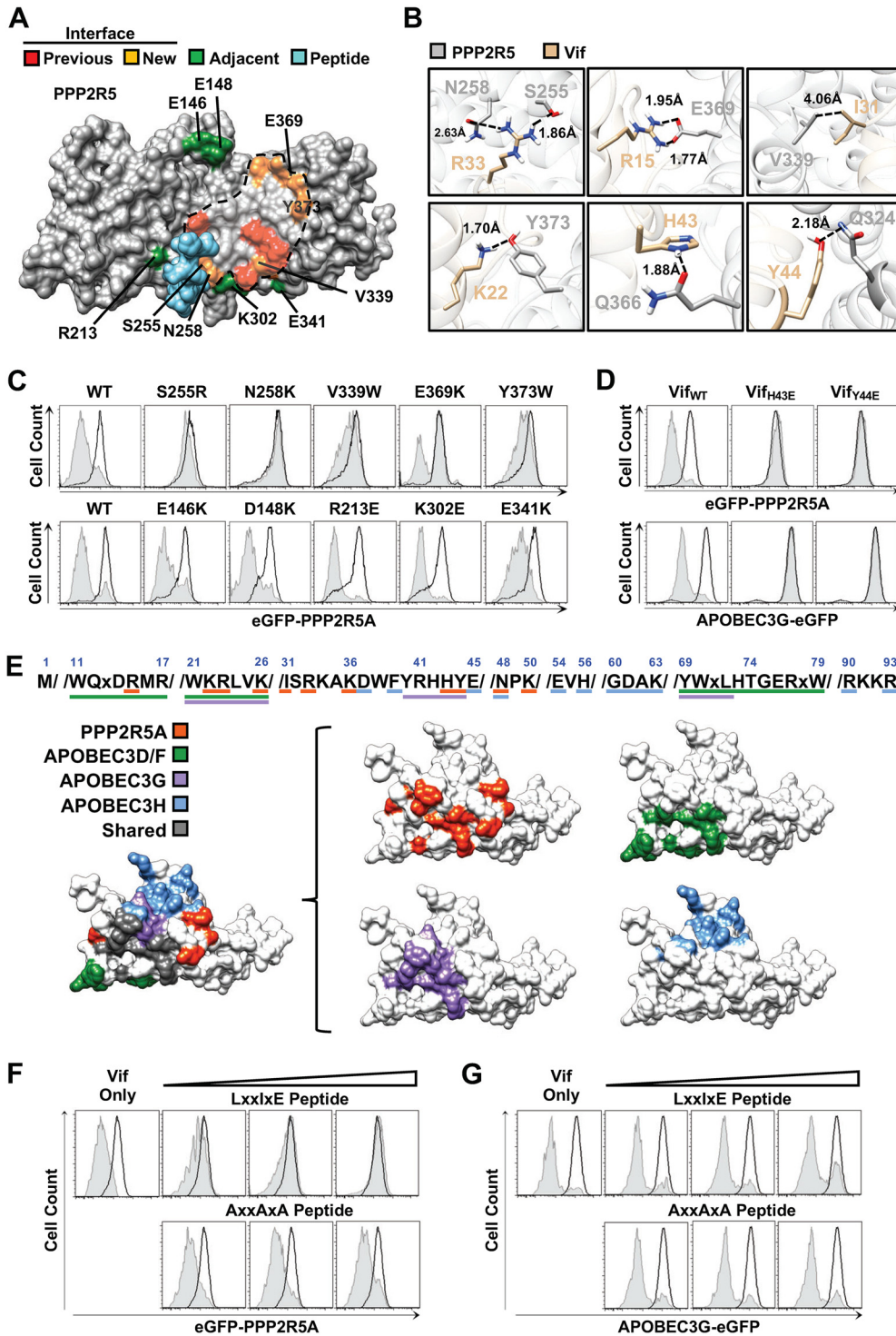


**FIG 2** Testing the Vif/PPP2R5 model. (A) Depiction of novel interface and interface-adjacent amino acid residues selected for validation. The LXXIXE inhibitory peptide is depicted in the substrate-binding cleft based on previously solved costructures (PDB codes 5SW9 and 5K6S). (B) Newly identified amino acid pairings between Vif and PPP2R5 within the protein-protein interface. (C) Flow cytometry histogram profiles from transient expression of wild-type Vif in 293T cell lines stably expressing PPP2R5A or mutant derivatives. (D) Flow cytometry histogram profiles from transient expression of the indicated Vif variants in 293T cell lines stably expressing PPP2R5A or APOBEC3G. (E) Amino acid sequence and surface models of IIB Vif highlighting residues required for PPP2R5A, APOBEC3D/F, APOBEC3G, or APOBEC3H degradation (“shared” indicates residues required for degradation of 2 or more substrates). (F and G) Flow cytometry histogram profiles from transient coexpression of wild-type Vif with either the LXXIXE or AXXAXA inhibitor peptides in cell lines stably expressing the indicated protein.

interface had a negligible impact on Vif-mediated degradation of PPP2R5A (Fig. 2A and C, bottom histograms).

A majority of the Vif surface highlighted by the PPD structural model has been characterized previously by mutagenesis and PPP2R5A degradation assays (Fig. 1A and B) (21); however, the model identified additional Vif residues, His43 and Tyr44, as being part of the interface. Because these Vif residues were predicted to form electrostatic interactions with their PPP2R5A counterparts (Fig. 1B), negatively charged amino acid residues were introduced at these positions and degradation of PPP2R5A and APOBEC3G was assessed (Fig. 2D). Both Vif mutants failed to degrade either substrate, which further supports the PPD structural model and previous results indicating that these residues are required for APOBEC3G degradation (23–25). In general, these findings support the model that Vif recognizes cellular substrates using largely distinct surfaces, with only partially overlapping amino acid residues (Fig. 2E) (26–28).

To independently test the Vif/PPP2R5 model, a series of experiments were done with a previously characterized high-affinity peptide inhibitor. This peptide contains a conserved LXXIXE motif that directly binds the substrate recognition region of PPP2R5 proteins and thereby effectively outcompetes interactions with substrates (Fig. 2A) (17, 20, 29). Cotransfection of a plasmid expressing 4 tandem copies of this inhibitory peptide caused a dose-dependent inhibition of Vif-mediated degradation of PPP2R5A (Fig. 2F). However, when a control plasmid encoding an AXXAXA motif was coexpressed with Vif, degradation of PPP2R5A was unaffected at all concentrations tested (Fig. 2F). Importantly, coexpression of either wild-type or alanine peptides with Vif had no effect on APOBEC3G degradation (Fig. 2G). These separation-of-function results indicate that the inhibitory peptide is specific to the Vif/PPP2R5 interaction and provides additional support for the structural model, since peptide binding would occlude residues Glu251, Ser255, and Asn258, which are required for Vif-mediated degradation of PPP2R5A (Fig. 2A and C).

**Vif concurrently degrades PPP2R5A and APOBEC3G substrates.** While the APOBEC3 surfaces recognized by Vif have been well characterized by genetic studies (Fig. 3A) (for a review, see reference 26), the kinetics of Vif-mediated degradation for a single substrate, or for concurrent degradation of multiple substrates, are poorly understood. Because both the Vif-PPP2R5 and Vif-APOBEC3 interaction surfaces are largely electrostatic (Fig. 3A), we investigated the kinetics of PPP2R5 degradation in comparison to the canonical Vif substrate APOBEC3G.

To establish degradation kinetics, we generated a HeLa cell line stably expressing both eGFP-APOBEC3G and PPP2R5A tagged with blue fluorescent protein (BFP) at near-physiologic levels and assessed Vif-mediated degradation in real time (Fig. 3B and C). Cells were infected at a low multiplicity of infection ( $<0.05$ ) with virus expressing either IIIIB Vif or a Vif mutant that cannot engage the E3-ubiquitin ligase complex (SLQ to AAA) (30, 31), and substrate abundance was monitored in real time (Movies S1 and S2). To track the progress of infection, *nef* was replaced with the mCherry gene to monitor long terminal repeat (LTR) activity and correlate loss of substrate abundance with the rate of infection establishment. Under these conditions, the half-life of APOBEC3G was estimated to be  $\sim 4$  h, and surprisingly, the half-life of PPP2R5A was only  $\sim 2$  h longer (fluorescence images in Fig. 3D and quantification in Fig. 3E). As a control, cells infected with virus expressing degradation-defective Vif displayed no changes in abundance of either APOBEC3G or PPP2R5A (fluorescence images in Fig. 3F and quantification in Fig. 3G). These observations indicate that Vif has a similar real-time preference for APOBEC3G and PPP2R5A as substrates in living cells and that functional Vif complexes are likely to concurrently degrade both substrates. However, it is important to emphasize that a single Vif complex is unlikely to accommodate both substrates at the same time, because a bound substrate would physically impede another from being engaged (Fig. 2E and 3A).

**PPP2R5 degradation activity in patient-derived Vif isolates.** Previous functional analyses of Vif sequences have established that APOBEC3G degradation is a highly

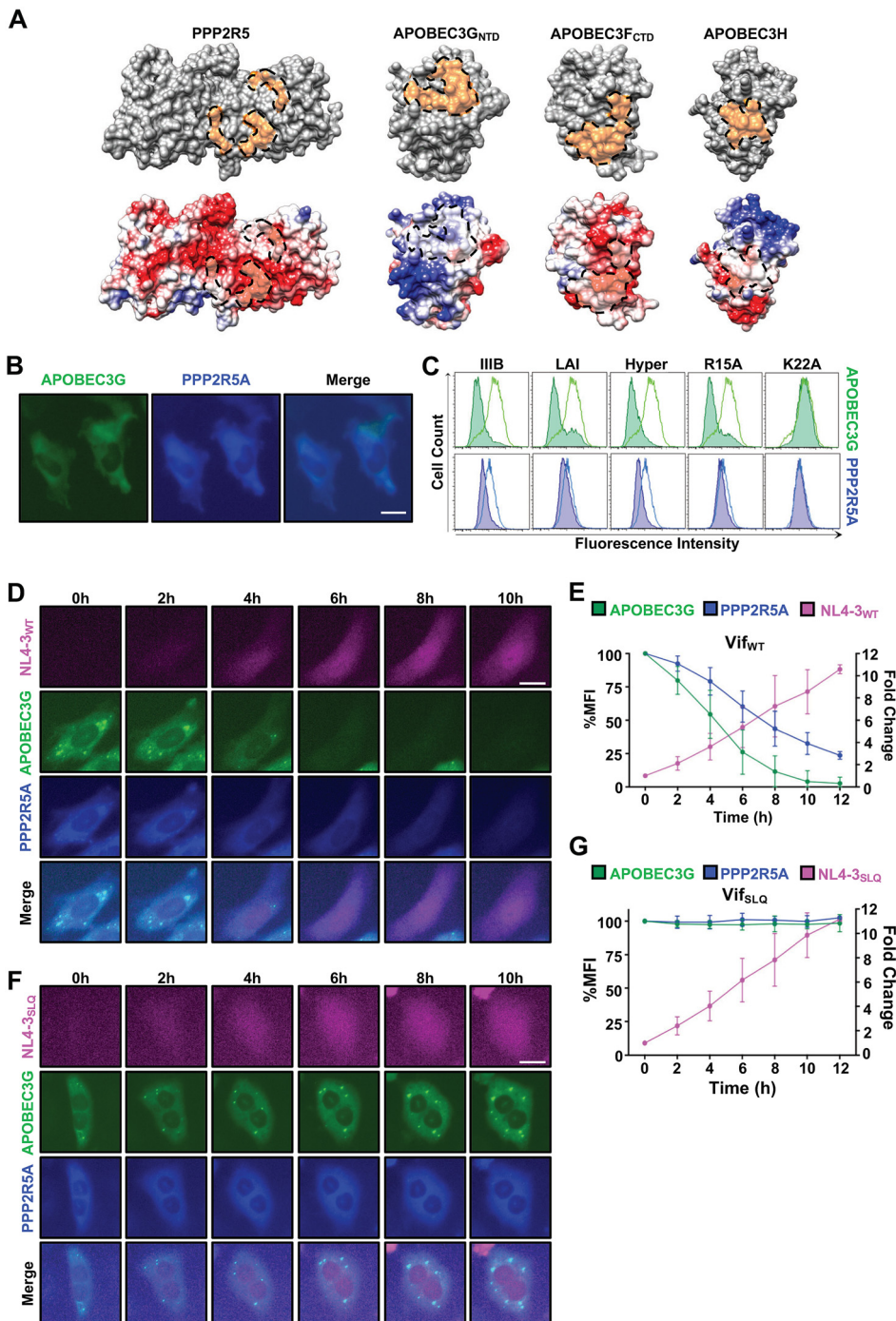


**FIG 3** Live cell degradation kinetics of PPP2R5A and APOBEC3G. (A) PPP2R5 and APOBEC3 surfaces (top) and electrostatic potential maps (bottom) of amino acid residues required for Vif-mediated degradation. (B) Fluorescence microscopy images of HeLa cells stably expressing both eGFP-APOBEC3G and BFP-PPP2R5A (bar = 20  $\mu$ m). (C) Flow cytometry histogram profiles from transient expression of the indicated Vif variants in HeLa cells stably expressing eGFP-APOBEC3G and BFP-PPP2R5A. (D and F) Images of dual-fluorescence HeLa cells infected with HIV-1 expressing either wild-type or SLQ-AAA Vif at the indicated time points (bar = 20  $\mu$ m). (E and G) Quantification of mean fluorescence intensity (MFI) from dual-fluorescence cells infected with wild-type or SLQ-AAA Vif (25 cells per condition).

conserved activity invariably observed in the Vif proteins of nearly all laboratory and clinical isolates (12, 32–34). In comparison, PPP2R5 degradation and G<sub>2</sub>/M arrest activities have not been as thoroughly characterized and are evidenced for some Vif isolates but not others (10, 12, 14, 21). To more comprehensively investigate the

potential conservation of the Vif/PPP2R5 interaction in a relevant context, a panel of patient-derived Vif isolates was studied to directly assess PPP2R5A degradation activity. In addition, a previous study had proposed a model in which the Vif amino acid residues required for G<sub>2</sub>/M cell cycle arrest partially overlap the residues required for degradation of APOBEC3H and, consequently, Vif could not engage in both activities simultaneously (Fig. 2E and 4A) (12). Therefore, we also assessed the ability of these patient-derived Vif isolates to degrade APOBEC3H (haplotype II).

Using samples and data from a previously characterized cohort of serodiscordant couples (35), two questions were addressed: (i) how prevalent is PPP2R5 degradation activity? and (ii) are PPP2R5 and APOBEC3H degradation activities mutually exclusive? Vif sequences were obtained by amplification of HIV-1 nucleic acids isolated from patient sera, and *APOBEC3H* genotypes were determined from amplification of genomic DNA from dried blood spots (36). All samples were Sanger sequenced and stratified into groups based on transmission outcome and *APOBEC3H* genotype (Fig. 4B).

Vif sequences were isolated from 15 patients where transmission had occurred (122 sequences) and 18 patients where transmission had not occurred (139 sequences), and allele frequencies were assessed at each amino acid position known to be important for Vif-mediated degradation of PPP2R5A (Fig. 1B and 4C) (21). Several patient samples were selected for further investigation based on their *APOBEC3H* genotype as depicted in Fig. 4B. To directly test activity, patient-derived Vif isolates were expressed transiently in 293T cell lines stably expressing fluorescently tagged PPP2R5A, APOBEC3H (haplotype II), or APOBEC3G, and degradation efficiency was assessed (Fig. 4D and E; protein expression was verified by immunoblotting [data not shown]). As controls, Vif isolates from IIB, LAI, and a hyper-functional Vif variant were included for comparison. The hyper-functional Vif variant was constructed previously based on patient-derived Vif alleles with strong APOBEC3H degradation activity (37). Roughly half of the Vif isolates from nontransmitted and transmitted virus showed activity against PPP2R5A, about a third showed activity against APOBEC3H, and almost all could efficiently degrade APOBEC3G (Fig. 4C; representative histograms are presented in Fig. 4D and E). Additionally, several of the isolates were able to efficiently degrade both PPP2R5A and APOBEC3H with no significant correlation between these activities among the isolates tested (Spearman correlation = -0.04;  $P = 0.798$ ). These results indicated that APOBEC3H and PPP2R5A degradation activities are not mutually exclusive in patients (Fig. 4E, box).

## DISCUSSION

While Vif's canonical role in antagonism of APOBEC3s has been studied extensively, its function in G<sub>2</sub>/M cell cycle arrest is less well characterized. Our group recently discovered that degradation of PPP2R5 phosphoregulators is required to induce G<sub>2</sub>/M arrest and demonstrated that this linkage is present in several common HIV-1 subtypes worldwide (21). Here, a Vif/PPP2R5 complex was investigated using protein-protein docking, targeted mutagenesis, and a peptide inhibitor that mimics physiologic PPP2R5 phosphatase substrates to probe the surface required for Vif-mediated degradation. The broader significance of this interaction was explored by interrogating a panel of patient-derived Vif isolates to establish that this activity is present in roughly half of the patient isolates tested. In addition, live-cell imaging studies revealed that the half-life of PPP2R5A is only ~2 h longer than that of APOBEC3G. Combined, the data from these studies indicated that PPP2R5 degradation and corresponding global changes in the cellular phosphoproteome are likely to occur rapidly following infection.

The structural model presented here builds on previous observations that the Vif/PPP2R5 interface is mediated primarily through electrostatic interactions (Fig. 1) (21). Of the 9 novel residues identified from the Vif/PPP2R5 model, 7 are either polar or charged amino acid residues (for Vif, His43 and Tyr44; for PPP2R5, Ser255, Asn258, Gln324, Gln366, Glu369, and Tyr373). Generating charge swap substitutions at several of these positions inhibited Vif's ability to degrade these PPP2R5A substrates (Fig. 2C and D). Importantly, generating similar substitutions at positions predicted to be

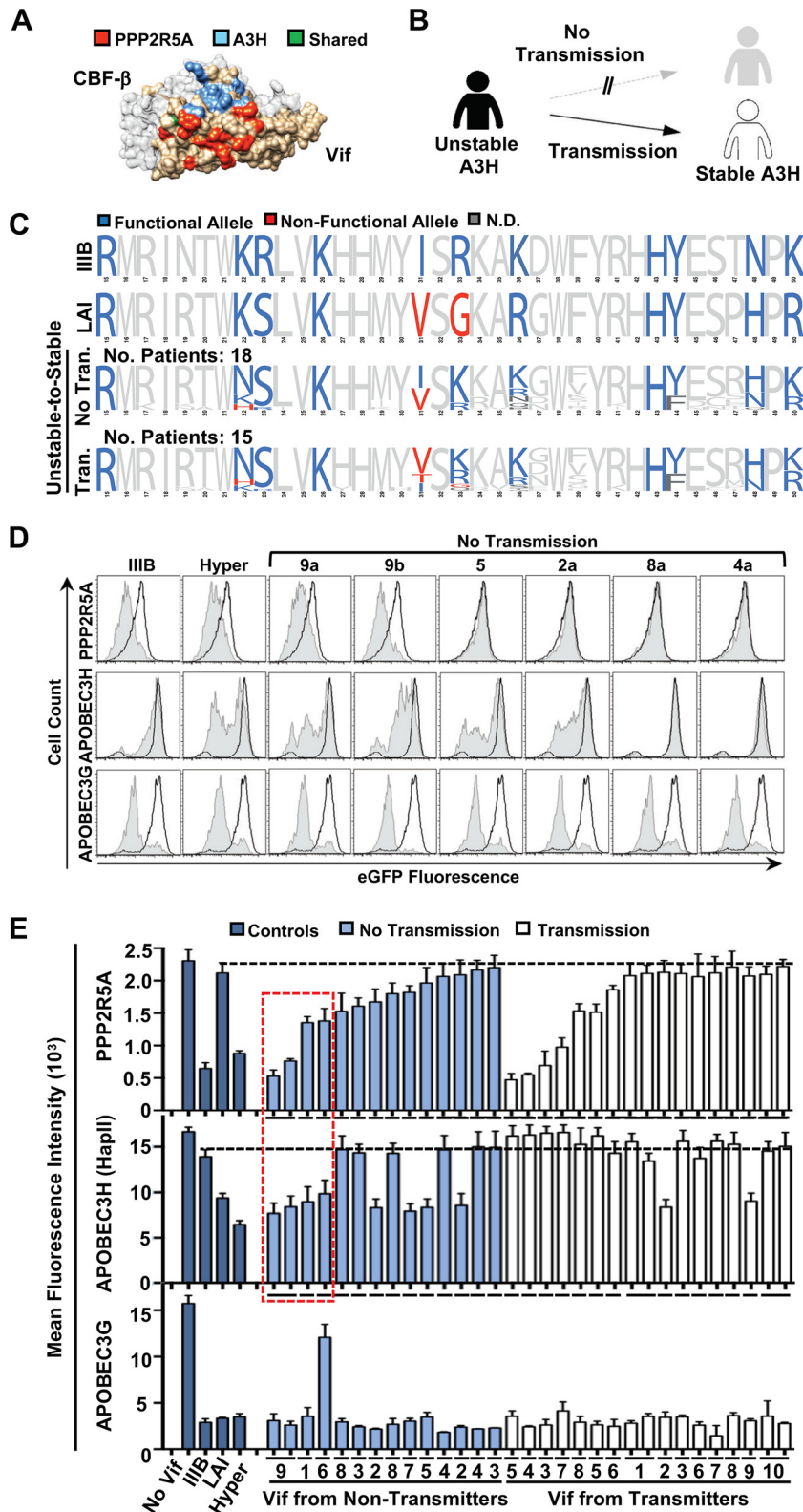


**FIG 4** Vif-induced degradation of PPP2R5A and APOBEC3H is not a mutually exclusive activity. (A) Surface model of Vif/CBF- $\beta$  highlighting residues required for PPP2R5A or APOBEC3H degradation. (B) Schematic of patient samples used in this study. (C) Sequence logos for the indicated patient-derived Vif sequences with IIIb Vif and LAI Vif shown for comparison. The number of patients is indicated, and 6 to 10 Vif sequences were analyzed from each patient. (D) Flow cytometry histogram profiles from transient expression of the indicated patient-derived Vif isolates in 293T cell lines stably expressing the indicated protein. (E) Flow cytometry results for transient expression of the indicated control and patient-derived

(Continued on next page)



immediately adjacent to the Vif/PPP2R5 interface had almost no impact on degradation (Fig. 2C). Furthermore, expression of a peptide that mimics natural PPP2R5 targets (20, 29, 38) robustly inhibited Vif-mediated degradation of PPP2R5A but not APOBEC3G (Fig. 2F and G).

Crystallographic studies of several different peptides bound to PPP2R5s have determined that the preferred LXXIXE target motif binds in an extended conformation between HEAT repeats 3 and 4 (Fig. 2A) (17, 20, 29). The LXXIXE motif interacts with two discrete helical surfaces that are conserved among PPP2R5 proteins. Motif binding requires interactions with specific residues across the helical surfaces, most notably the hydrophobic residues Ile256 and Phe260 and the hydrophilic residue Lys265 (17). Therefore, the most likely mode of LXXIXE peptide inhibition of Vif-induced PPP2R5A degradation is through occlusion of residues Glu251, Ser255, and Asn258, which are required for degradation (Fig. 1B and 2A and C). Interestingly, a recent study determined that PPP2R5 substrate recognition is enhanced by electrostatic interactions that occur adjacent to the LXXIXE binding cleft. Recognition of the PPP2R5 substrate KIF4A is enhanced through electrostatic interactions between positively charged KIF4A residues and highly conserved negatively charged PPP2R5 residues (39). Two of these PPP2R5 residues, Glu335 and Asp338, are also required for Vif-mediated degradation of PPP2R5 family members (Fig. 1) (21). Taken together, these findings provide further support for the PPD structural model of the Vif/PPP2R5 cocomplex.

The observation that Vif degrades PPP2R5A with kinetics comparable to those for APOBEC3G was surprising given that APOBEC3G is considered the most ancient and antagonistic Vif substrate (40, 41). Previous studies using pulse-chase or fluorescence microscopy experiments on cells infected with Vif-proficient HIV-1 have established that APOBEC3G has a half-life of roughly 4 to 8 h after initial detection of viral proteins (42–45). In support of these previous findings, our live-cell imaging studies established similar kinetics for APOBEC3G degradation and are the first to report degradation kinetics for PPP2R5 substrates and to assess concurrent degradation of distinct Vif substrates in the same cell (Fig. 3). Surprisingly, the half-life of PPP2R5A is only ~2 h longer than that of APOBEC3G, consistent with observations that a rapid remodeling of the host phosphoproteome occurs in HIV-1-infected cells (14, 15).

To address the broader significance of the Vif/PPP2R5 interaction, a panel of patient-derived Vif isolates were examined to determine the prevalence of this activity in patients (Fig. 4). Roughly half of the patient samples displayed robust activity against PPP2R5A, regardless of transmissibility (Fig. 4E). Interestingly, PPP2R5 proteins have been shown to be targets of other viral pathogens and, in the case of Ebola virus and human T-lymphotropic virus (HTLV), PPP2R5 proteins are required for efficient virus replication (38, 46, 47). Ebola virus nucleoprotein recruits a PPP2R5 protein through an LXXIXE motif to dephosphorylate the viral VP30 protein, which promotes transcription of the viral genome and subsequent infection (38). Likewise, the integrase proteins from HTLV-1, HTLV-2, and bovine leukemia virus require PPP2R5C for efficient strand transfer activity (46). Interestingly, HTLV-1 integrase was shown to bind the patch of conserved residues on PPP2R5C that physiologic targets bind, similar to our Vif/PPP2R5 co-complex (47). Taken together, these findings suggest that manipulation of PPP2R5s may be a conserved function of diverse viral families.

## MATERIALS AND METHODS

**Cohorts and human subjects.** Blood spot and plasma samples associated with both partners of HIV-1 transmitting and nontransmitting couples from the Partners in Prevention HSV/HIV Transmission Study were used for this analysis (35). This clinical trial of herpes simplex virus 2 (HSV-2) suppression with acyclovir versus placebo in HSV-2 and HIV-1 dually infected persons recruited in seven sub-Saharan African countries to reduce transmission to their HIV-uninfected heterosexual partner found no reduction

### FIG 4 Legend (Continued)

Vif proteins in 293T cell lines stably expressing the indicated protein. Patient identification codes are shown below the corresponding sample, with the dashed red box indicating Vif isolates that could efficiently degrade both PPP2R5A and APOBEC3H.

in HIV-1 transmission risk between the acyclovir and placebo arms (Clinicaltrials.gov no. NCT00194519). Only samples collected from individuals who provided consent for future research on HIV and HIV-related infections were used for our analysis. All study documents were reviewed and approved by appropriate institutional review boards.

**Cell lines and culture conditions.** HEK 293T and HeLa cells were maintained in Dulbecco's modified Eagle medium (DMEM) (HyClone, South Logan, UT) supplemented with 10% fetal bovine serum (FBS) (Gibco, Gaithersburg, MD) and 0.5% penicillin-streptomycin (50 U). 293T cells were transfected with Transit LTI (Mirus, Madison, WI) according to the manufacturer's protocol. Generation of PPP2R5A and APOBEC3G cell lines has been described (21). To generate stable APOBEC3H, PP2C $\alpha$ , PPP2R1 $\alpha$ , and PPP2R1 $\beta$  cells, viruses were produced from 293T cells transfected with a pQCXIH retroviral expression vector containing the appropriate expression cassette, a murine leukemia virus (MLV) GagPol packaging vector, and a vesicular stomatitis virus G (VSV-G) vector. Medium was harvested 48 h posttransfection, frozen at  $-80^{\circ}\text{C}$  for 4 to 6 h, thawed, centrifuged at  $1,500 \times g$ , and combined with fresh 293T cells. To generate pure cell populations, samples were treated with hygromycin B (Sigma;  $200 \mu\text{g/ml}$ ) 48 h posttransduction. The same procedure was followed for generation of the dual eGFP-APOBEC3G/BFP-PPP2R5A HeLa cell line with the modification that cells were coinfecting with virus carrying the respective expression cassette and treated with both puromycin (Sigma;  $1 \mu\text{g/ml}$ ) and hygromycin B (Sigma;  $200 \mu\text{g/ml}$ ) 48 h posttransduction.

**Plasmids and cloning.** All APOBEC3 and PPP2R5A expression plasmids used in this study were cloned into the pQCXIH retroviral expression vector (21). PPP2R5A and Vif point mutants were generated by PCR amplification using Phusion high-fidelity DNA polymerase (NEB, Ipswich, MA) and overlapping PCR to introduce the desired mutations. To generate the yellow fluorescent protein (YFP) wild-type and -alanine inhibitor peptide expression cassettes, gene blocks were ordered from Integrated DNA Technologies and cloned into pcDNA 5TO expression vectors. Patient-derived Vif isolates were cloned into an existing lentiviral expression vector (21). All constructs were confirmed by restriction digestion and Sanger sequencing.

**Isolation of patient Vif sequences.** Isolation of patient-derived Vif isolates and APOBEC3H genotyping have been described (36). Briefly, patient serum was centrifuged at  $21,000 \times g$  for 75 min to concentrate viral particles. After centrifugation, a QIAamp viral RNA preparation minikit was used to recover RNA following the manufacturer's protocol. To generate cDNA,  $3 \mu\text{l}$  of the purified RNA was combined with  $7.5 \mu\text{l}$  diethyl pyrocarbonate (DEPC)-treated  $\text{H}_2\text{O}$  and  $2.5 \mu\text{l}$  of a  $20 \mu\text{M}$  reverse primer specific to the HIV-1 genome (primer sequence,  $5'$ -GGTACCCATAATAGACTGTRACCCACAA- $3'$ ). This mixture was incubated at  $65^{\circ}\text{C}$  for 10 min, chilled on ice for at least 1 min, and then combined with the following:  $4 \mu\text{l}$   $5\times$  reverse transcription [RT] buffer,  $0.5 \mu\text{l}$  RNase inhibitor,  $2 \mu\text{l}$  10 mM deoxynucleoside triphosphate [dNTP] mix, and  $0.5 \mu\text{l}$  Transcriptor RT. The complete mixture was incubated at  $55^{\circ}\text{C}$  for 30 min and then  $85^{\circ}\text{C}$  for 5 min. To isolate Vif sequences, the cDNA was amplified using nested primers that flanked the *int/vif/vpr* gene cassette, cloned into a pJET blunt 2.0 vector, and subjected to Sanger sequencing.

**APOBEC3H genotyping.** To isolate gDNA from dried blood spots, three filter paper punch-outs containing the dried blood were soaked in  $40 \mu\text{l}$  Tris-EDTA buffer and incubated at  $37^{\circ}\text{C}$  overnight. Genomic DNA was isolated from blood using a DNeasy blood and tissue kit (Qiagen, Valencia, CA, USA). For genotyping, exon 2 or 3 of APOBEC3H was amplified from genomic DNA (gDNA) isolations to determine the patient genotype. To amplify exon 2, the following primer pair was used: forward,  $5'$ -CCGAAACATTCGCTTACAG- $3'$ , and reverse,  $5'$ -AACTGGGCCACTCAGATCC- $3'$ . To amplify exon 3, the following primer pair was used: forward,  $5'$ -GAAAAGTGCATGCAGAAATTTGCTT- $3'$ , and reverse,  $5'$ -CTGGGAAGCCCATGACCTCC- $3'$ . The following cycling conditions were used to amplify these gene segments:  $94^{\circ}\text{C}$  for 5 min, 13 cycles of  $94^{\circ}\text{C}$  for 45 s,  $68^{\circ}\text{C}$  for 30 s, and  $72^{\circ}\text{C}$  for 1.5 min, and then 22 cycles of  $94^{\circ}\text{C}$  for 45 s. The PCR products were then purified using an enzymatic cleanup protocol including  $4.9 \mu\text{l}$  of DEPC  $\text{H}_2\text{O}$ ,  $0.0125 \mu\text{l}$  exonuclease I (NEB), and  $0.125 \mu\text{l}$  of rShrimp alkaline phosphatase. To each PCR mixture,  $5 \mu\text{l}$  of this mix was added, and the mixtures were incubated at  $37^{\circ}\text{C}$  for 30 min and then heat inactivated at  $95^{\circ}\text{C}$  for 10 min. PCR products were then subjected directly to Sanger sequencing to determine the APOBEC3H genotypes.

**Protein-protein docking.** We used the ClusPro protein-protein docking web server (48) to generate 30 models for the Vif/CBF- $\beta$ /PPP2R5 complex using the balanced scoring method. The atomic coordinates of Vif/CBF- $\beta$  complex and PPP2R5 protein were taken from PDB structures 4N9F (chains A and B) and 2IAE (chain B), respectively. Based on our prior mutagenesis studies (21), residues Arg15, Lys22, Arg23, Lys26, Arg33, and Lys36 on Vif and residues Glu251, Glu301, Glu335, and Asp338 on PPP2R5 were used as anchor points for the docking. After analyzing all 30 computational models for predicted interfaces, and especially focusing on the salt-bridge interactions between the Vif and PPP2R5 proteins, we selected one optimal model (Fig. 1).

**Vif substrate degradation assays.** For all degradation assays, 293T cell lines stably expressing the fluorescently tagged protein were plated into 12-well plates at a seeding density of approximately 250,000 cells per well. The next day, cells were transfected with 250 ng of the relevant Vif construct and incubated for 48 h. After 48 h posttransfection, cells were harvested using phosphate-buffered saline (PBS)-EDTA and collected for both flow cytometry (as indicated in the figure legends) and immunoblotting (data not shown) to confirm Vif expression. To determine relative eGFP loss, samples were analyzed via flow cytometry. Sample populations were first separated by forward and side scatter to isolate live singular events. After the live/single-event population was isolated, the mCherry-positive population was isolated and the eGFP fluorescence intensity was assessed. The resulting histograms or bar graphs presented here display the eGFP fluorescence profile of the isolated mCherry-positive population. For

inhibitor studies, various cell lines were cotransfected with a BFP-2A-Vif expression vector and a four-peptide-expressing mCherry vector that contained either the wild-type LXXIXE or mutant AXXAXA sequence.

**Live-cell imaging microscopy.** To generate the virus used for live-cell imaging experiments, approximately 500,000 293T cells were plated on a 6-well culture plate and allowed to adhere overnight. The next day, cells were transfected with 900 ng of an HIV-1 *vpr*, *vpu*, *env*, and *nef*-deficient mCherry reporter virus (where *nef* has been replaced with mCherry) and 150 ng of a VSV-G expression construct. Medium was harvested 48 h posttransfection and frozen for at least 8 h at  $-80^{\circ}\text{C}$ , and then the virus titer was determined on fresh HeLa cells using increasing increments of supernatant. After 48 h, mCherry-positive cells were analyzed using flow cytometry to determine optimal multiplicity of infection.

For imaging studies, HeLa cells stably expressing eGFP-APOBEC3G and BFP-PPP2R5A were plated on an 8-well microslide (Ibidi) and allowed to adhere overnight. The next day, cells were transduced with virus containing one of the Vif variants and imaged using a Nikon Inverted Ti-E deconvolution microscope with images acquired every 60 min over a time course of roughly 12 h. All images were processed and fluorescence intensity was quantified using Fiji/ImageJ2.

**Quantification and statistical analysis.** All flow cytometry data and associated histogram profiles were generated using FlowJo 8.8.6 software. The data shown are representative results from one of three independent experiments. Bar graphs were generated using GraphPad Prism 6 software. The protein complex depicted in Fig. 1B and C were generated using Chimera protein modeling software. Error bars generated in Fig. 3 and 4 were calculated based on standard errors of the means (SEM) of the data obtained from three independent sample sets.

## SUPPLEMENTAL MATERIAL

Supplemental material is available online only.

**SUPPLEMENTAL FILE 1**, AVI file, 4.1 MB.

**SUPPLEMENTAL FILE 2**, AVI file, 3.1 MB.

**SUPPLEMENTAL FILE 3**, PDF file, 0.02 MB.

## ACKNOWLEDGMENTS

This work was supported by NIAID R37-AI064046 (to R.S.H.). D.J.S. received salary support from the University of Minnesota Craniofacial Research Training (MinnCResT) program (NIH T90DE022732) and from an NIAID K99/R00 transition award (K99-AI147811). R.S.H. is the Margaret Harvey Schering Land Grant Chair for Cancer Research, a Distinguished University McKnight Professor, and an Investigator of the Howard Hughes Medical Institute.

R.S.H. is a cofounder, shareholder, and consultant of ApoGen Biotechnologies Inc. R.E.A. is a cofounder, is on the Scientific Advisory Board and has equity interest in Actavalon, Inc. The other authors declare no competing financial interests.

D.J.S. and R.S.H. led the project. D.J.S. made all DNA constructs and performed most of the experiments. Ö.D., N.A.T., and R.E.A. generated the Vif/PPP2R5 structural model, J.L.M. contributed to immunoblots, J.W. and J.R.L. contributed to isolating patient-derived Vif sequences, J.T.B. contributed to live-cell imaging studies, and W.L.B. contributed to project logistics. D.J.S. and R.S.H. drafted the manuscript, and all authors contributed to revisions.

## REFERENCES

- Desimie BA, Delviks-Frankenberry KA, Burdick RC, Qi D, Izumi T, Pathak VK. 2014. Multiple APOBEC3 restriction factors for HIV-1 and one Vif to rule them all. *J Mol Biol* 426:1220–1245. <https://doi.org/10.1016/j.jmb.2013.10.033>.
- Harris R, Dudley J. 2015. APOBECs and virus restriction. *Virology* 479–480:131–145. <https://doi.org/10.1016/j.virol.2015.03.012>.
- Malim MH, Emerman M. 2008. HIV-1 accessory proteins—ensuring viral survival in a hostile environment. *Cell Host Microbe* 3:388–398. <https://doi.org/10.1016/j.chom.2008.04.008>.
- Simon V, Bloch N, Landau N. 2015. Intrinsic host restrictions to HIV-1 and mechanisms of viral escape. *Nat Immunol* 16:546–553. <https://doi.org/10.1038/ni.3156>.
- Guo Y, Dong L, Qiu X, Wang Y, Zhang B, Liu H, Yu Y, Zang Y, Yang M, Huang Z. 2014. Structural basis for hijacking CBF- $\beta$  and CUL5 E3 ligase complex by HIV-1 Vif. *Nature* 505:229–233. <https://doi.org/10.1038/nature12884>.
- Jäger S, Kim DY, Hultquist JF, Shindo K, LaRue RS, Kwon E, Li M, Anderson BD, Yen L, Stanley D, Mahon C, Kane J, Franks-Skiba K, Cimermanic P, Burlingame A, Sali A, Craik CS, Harris RS, Gross JD, Krogan NJ. 2011. Vif hijacks CBF- $\beta$  to degrade APOBEC3G and promote HIV-1 infection. *Nature* 481:371–375. <https://doi.org/10.1038/nature10693>.
- Holmes RK, Koning FA, Bishop KN, Malim MH. 2007. APOBEC3F can inhibit the accumulation of HIV-1 reverse transcription products in the absence of hypermutation. Comparisons with APOBEC3G. *J Biol Chem* 282:2587–2595. <https://doi.org/10.1074/jbc.M607298200>.
- Newman EN, Holmes RK, Craig HM, Klein KC, Lingappa JR, Malim MH, Sheehy AM. 2005. Antiviral function of APOBEC3G can be dissociated from cytidine deaminase activity. *Curr Biol* 15:166–170. <https://doi.org/10.1016/j.cub.2004.12.068>.
- DeHart JL, Zimmerman ES, Ardon O, Monteiro-Filho CM, Argañaraz ER, Planelles V. 2007. HIV-1 Vpr activates the G2 checkpoint through manipulation of the ubiquitin proteasome system. *Virology* 457:4–57. <https://doi.org/10.1186/1743-422X-4-57>.
- Izumi T, Ito K, Matsui M, Shirakawa K, Shinohara M, Nagai Y, Kawahara M,

- Kobayashi M, Kondoh H, Misawa N, Koyanagi Y, Uchiyama T, Takaori-Kondo A. 2010. HIV-1 viral infectivity factor interacts with TP53 to induce G2 cell cycle arrest and positively regulate viral replication. *Proc Natl Acad Sci U S A* 107:20798–20803. <https://doi.org/10.1073/pnas.1008076107>.
11. Sakai K, Dimas J, Lenardo MJ. 2006. The Vif and Vpr accessory proteins independently cause HIV-1-induced T cell cytopathicity and cell cycle arrest. *Proc Natl Acad Sci U S A* 103:3369–3374. <https://doi.org/10.1073/pnas.0509417103>.
  12. Zhao K, Du J, Rui Y, Zheng W, Kang J, Hou J, Wang K, Zhang W, Simon VA, Yu XF. 2015. Evolutionarily conserved pressure for the existence of distinct G2/M cell cycle arrest and A3H inactivation functions in HIV-1 Vif. *Cell Cycle* 14:838–847. <https://doi.org/10.1080/15384101.2014.1000212>.
  13. Du J, Rui Y, Zheng W, Li P, Kang J, Zhao K, Sun T, Yu XF. 2019. Vif-CBF $\beta$  interaction is essential for Vif-induced cell cycle arrest. *Biochem Biophys Res Commun* 511:910–915. <https://doi.org/10.1016/j.bbrc.2019.02.136>.
  14. Greenwood EJ, Matheson NJ, Wals K, van den Boomen DJ, Antrobus R, Williamson JC, Lehner PJ. 2016. Temporal proteomic analysis of HIV infection reveals remodelling of the host phosphoproteome by lentiviral Vif variants. *Elife* 5:e18296. <https://doi.org/10.7554/eLife.18296>.
  15. Naamati A, Williamson JC, Greenwood EJ, Marelli S, Lehner PJ, Matheson NJ. 2019. Functional proteomic atlas of HIV infection in primary human CD4+ T cells. *Elife* 8:e41431. <https://doi.org/10.7554/eLife.41431>.
  16. McCright B, Rivers AM, Audlin S, Virshup DM. 1996. The B56 family of protein phosphatase 2A (PP2A) regulatory subunits encodes differentiation-induced phosphoproteins that target PP2A to both nucleus and cytoplasm. *J Biol Chem* 271:22081–22089. <https://doi.org/10.1074/jbc.271.36.22081>.
  17. Wang X, Bajaj R, Bollen M, Peti W, Page R. 2016. Expanding the PP2A interactome by defining a B56-specific SLiM. *Structure* 24:2174–2181. <https://doi.org/10.1016/j.str.2016.09.010>.
  18. Nilsson J. 2019. Protein phosphatases in the regulation of mitosis. *J Cell Biol* 218:395–409. <https://doi.org/10.1083/jcb.201809138>.
  19. Thompson JJ, Williams CS. 2018. Protein phosphatase 2A in the regulation of Wnt signaling, stem cells, and cancer. *Genes (Basel)* 9:121–131. <https://doi.org/10.3390/genes9030121>.
  20. Wang J, Wang Z, Yu T, Yang H, Virshup DM, Kops GJ, Lee SH, Zhou W, Li X, Xu W, Rao Z. 2016. Crystal structure of a PP2A B56-BubR1 complex and its implications for PP2A substrate recruitment and localization. *Protein Cell* 7:516–526. <https://doi.org/10.1007/s13238-016-0283-4>.
  21. Salamango DJ, Ikeda T, Moghadasi SA, Wang J, McCann JL, Serebrenik AA, Ebrahimi D, Jarvis MC, Brown WL, Harris RS. 2019. HIV-1 Vif triggers cell cycle arrest by degrading cellular PPP2R5 phospho-regulators. *Cell Rep* 29:1057–1065. <https://doi.org/10.1016/j.celrep.2019.09.057>.
  22. Hu Y, Desimie BA, Nguyen HC, Ziegler SJ, Cheng TC, Chen J, Wang J, Wang H, Zhang K, Pathak VK, Xiong Y. 2019. Structural basis of antagonism of human APOBEC3F by HIV-1 Vif. *Nat Struct Mol Biol* 26:1176–1183. <https://doi.org/10.1038/s41594-019-0343-6>.
  23. Russell RA, Pathak VK. 2007. Identification of two distinct human immunodeficiency virus type 1 Vif determinants critical for interactions with human APOBEC3G and APOBEC3F. *J Virol* 81:8201–8210. <https://doi.org/10.1128/JVI.00395-07>.
  24. Yamashita T, Kamada K, Hachio K, Adachi A, Nomaguchi M. 2008. Identification of amino acid residues in HIV-1 Vif critical for binding and exclusion of APOBEC3G/F. *Microbes Infect* 10:1142–1149. <https://doi.org/10.1016/j.micinf.2008.06.003>.
  25. Chen G, He Z, Wang T, Xu R, Yu XF. 2009. A patch of positively charged amino acids surrounding the human immunodeficiency virus type 1 Vif SLVx4Yx9Y motif influences its interaction with APOBEC3G. *J Virol* 83:8674–8682. <https://doi.org/10.1128/JVI.00653-09>.
  26. Azimi FC, Lee JE. 2020. Structural perspectives on HIV-1 Vif and APOBEC3 restriction factor interactions. *Protein Sci* 29:391–406. <https://doi.org/10.1002/pro.3729>.
  27. Feng Y, Baig TT, Love RP, Chelico L. 2014. Suppression of APOBEC3-mediated restriction of HIV-1 by Vif. *Front Microbiol* 5:450. <https://doi.org/10.3389/fmicb.2014.00450>.
  28. Ooms M, Letko M, Simon V. 2017. The structural interface between HIV-1 Vif and human APOBEC3H. *J Virol* 91:e02289-16. <https://doi.org/10.1128/JVI.02289-16>.
  29. Hertz EPT, Kruse T, Davey NE, López-Méndez B, Sigurðsson JO, Montoya G, Olsen JV, Nilsson J. 2016. A conserved motif provides binding specificity to the PP2A-B56 phosphatase. *Mol Cell* 63:686–695. <https://doi.org/10.1016/j.molcel.2016.06.024>.
  30. LaRue RS, Lengyel J, Jónsson SR, Andrésdóttir V, Harris RS. 2010. Lentiviral Vif degrades the APOBEC3Z3/APOBEC3H protein of its mammalian host and is capable of cross-species activity. *J Virol* 84:8193–8201. <https://doi.org/10.1128/JVI.00685-10>.
  31. Yu X, Yu Y, Liu B, Luo K, Kong W, Mao P, Yu XF. 2003. Induction of APOBEC3G ubiquitination and degradation by an HIV-1 Vif-Cul5-SCF complex. *Science* 302:1056–1060. <https://doi.org/10.1126/science.1089591>.
  32. Binka M, Ooms M, Steward M, Simon V. 2012. The activity spectrum of Vif from multiple HIV-1 subtypes against APOBEC3G, APOBEC3F, and APOBEC3H. *J Virol* 86:49–59. <https://doi.org/10.1128/JVI.06082-11>.
  33. Reddy K, Ooms M, Letko M, Garrett N, Simon V, Ndung'u T. 2016. Functional characterization of Vif proteins from HIV-1 infected patients with different APOBEC3G haplotypes. *AIDS* 30:1723–1729. <https://doi.org/10.1097/QAD.0000000000001113>.
  34. Baig TT, Feng Y, Chelico L. 2014. Determinants of efficient degradation of APOBEC3 restriction factors by HIV-1 Vif. *J Virol* 88:14380–14395. <https://doi.org/10.1128/JVI.02484-14>.
  35. Celum C, Wald A, Lingappa JR, Magaret AS, Wang RS, Mugo N, Mujugira A, Baeten JM, Mullins JI, Hughes JP, Bukusi EA, Cohen CR, Katabira E, Ronald A, Kiarie J, Farquhar C, Stewart GJ, Makhema J, Essex M, Were E, Fife KH, de Bruyn G, Gray GE, McIntyre JA, Manongi R, Kapiga S, Coetzee D, Allen S, Inambao M, Kayitenkore K, Karita E, Kanweka W, Delany S, Rees H, Vwalika B, Stevens W, Campbell MS, Thomas KK, Coombs RW, Morrow R, Whittington WL, McElrath MJ, Barnes L, Ridzon R, Corey L, Partners in Prevention HSV/HIV Transmission Study Team. 2010. Acyclovir and transmission of HIV-1 from persons infected with HIV-1 and HSV-2. *N Engl J Med* 362:427–439. <https://doi.org/10.1056/NEJMoa0904849>.
  36. Wang J, Land AM, Hoium BJ, Refsland EW, Luengas EM, Brown WL, Mackelprang RD, Emerman M, Lingappa J, Harris RS. The impact of stable and unstable APOBEC3H haplotypes on HIV-1 transmission. *J Int AIDS Society*, in process.
  37. Refsland EW, Hultquist JF, Luengas EM, Ikeda T, Shaban NM, Law EK, Brown WL, Reilly C, Emerman M, Harris RS. 2014. Natural polymorphisms in human APOBEC3H and HIV-1 Vif combine in primary T lymphocytes to affect viral G-to-A mutation levels and infectivity. *PLoS Genet* 10:e1004761. <https://doi.org/10.1371/journal.pgen.1004761>.
  38. Kruse T, Biedenkopf N, Hertz EPT, Dietzel E, Stalman G, López-Méndez B, Davey NE, Nilsson J, Becker S. 2018. The Ebola virus nucleoprotein recruits the host PP2A-B56 phosphatase to activate transcriptional support activity of VP30. *Mol Cell* 69:136–145. <https://doi.org/10.1016/j.molcel.2017.11.034>.
  39. Wang X, Garvanska DH, Nasa I, Ueki Y, Zhang G, Kettenbach AN, Peti W, Nilsson J, Page R. 2020. A dynamic charge-charge interaction modulates PP2A:B56 substrate recruitment. *Elife* 9:9e55966. <https://doi.org/10.7554/eLife.55966>.
  40. Zhang J, Webb DM. 2004. Rapid evolution of primate antiviral enzyme APOBEC3G. *Hum Mol Genet* 13:1785–1791. <https://doi.org/10.1093/hmg/ddh183>.
  41. Ortiz M, Bleiber G, Martinez R, Kaessmann H, Telenti A. 2006. Patterns of evolution of host proteins involved in retroviral pathogenesis. *Retrovirology* 3:11–18. <https://doi.org/10.1186/1742-4690-3-11>.
  42. Conticello SG, Harris RS, Neuberger MS. 2003. The Vif protein of HIV triggers degradation of the human antiretroviral DNA deaminase APOBEC3G. *Curr Biol* 13:2009–2013. <https://doi.org/10.1016/j.cub.2003.10.034>.
  43. Becker JT, Evans EL III, Benner BE, Fricke SL, Smith LE, Bates AE, Sherer NM. 2019. HIV-1 genome trafficking initiates APOBEC3G packaging in the cytosol. *bioRxiv* <https://www.biorxiv.org/content/10.1101/846105v1>.
  44. Holmes M, Zhang F, Bieniasz PD. 2015. Single-cell and single-cycle analysis of HIV-1 replication. *PLoS Pathog* 11:e1004961. <https://doi.org/10.1371/journal.ppat.1004961>.
  45. Sheehy AM, Gaddis NC, Malim MH. 2003. The antiretroviral enzyme APOBEC3G is degraded by the proteasome in response to HIV-1 Vif. *Nat Med* 9:1404–1407. <https://doi.org/10.1038/nm945>.
  46. Maertens GN. 2016. B<sup>2</sup>-protein phosphatase 2A is a functional binding partner of delta-retroviral integrase. *Nucleic Acids Res* 44:364–376. <https://doi.org/10.1093/nar/gkv1347>.
  47. Bhatt V, Shi K, Salamango DJ, Moeller NH, Pandey KK, Bera S, Bohl TE, Kunriawan F, Orellana K, Zhang W, Grandgenett DP, Harris RS, Sundborger-Lunna AC, Aihara H. 2020. Structural basis of host protein hijacking in human T-cell leukemia virus integration. *Nat Commun* 11:3121–3129. <https://doi.org/10.1038/s41467-020-16963-6>.
  48. Kozakov D, Hall DR, Xia B, Porter KA, Padhorna D, Yueh C, Beglov D, Vajda S. 2017. The ClusPro web server for protein-protein docking. *Nat Protoc* 12:255–278. <https://doi.org/10.1038/nprot.2016.169>.